Dynamically Tuneable Reflective Structural Coloration with Electroactive Conducting Polymer Nanocavities

ADVANCED MATERIALS
www.advmat.de

Dynamically Tuneable Reflective Structural Coloration with Electroactive Conducting Polymer Nanocavities

*Stefano Rossi, Oliver Olsson, Shangzhi Chen, Ravi Shanker, Debashree Banerjee, Andreas Dahlin, and Magnus P. Jonsson**

Dynamic control of structural colors across the visible spectrum with high brightness has proven to be a difficult challenge. Here, this is addressed with a tuneable reflective nano-optical cavity that uses an electroactive conducting polymer (poly(thieno[3,4-b]thiophene)) as spacer layer. Electrochemical doping and dedoping of the polymer spacer layer provides reversible tuning of the cavity's structural color throughout the entire visible range and beyond. Furthermore, the cavity provides high peak reflectance that varies only slightly between the reduced and oxidized states of the polymer. The results indicate that the polymer undergoes large reversible thickness changes upon redox tuning, aided by changes in optical properties and low visible absorption. The electroactive cavity concept may find particular use in reflective displays, by opening for tuneable monopixels that eliminate limitations in brightness of traditional subpixel-based systems.

1. Introduction

Displays form an integral part of modern society while at the same time they are responsible for a significant part of our energy consumption. The inevitable increasing global usage of displays further highlights the need for more energy-efficient and sustainable solutions. The limited room for further improvement of emissive displays motivates the development of a complementary energy-effective reflective-based technology.[1] Reflective displays, or electronic paper (e-paper), do not consume energy by producing and emitting light, but instead generate text and images by controlling the reflection of natural indoor or outdoor lighting, just as a piece of paper. Besides energy savings, e-paper has the added benefit of providing glare-free surfaces for which the visibility even improves in sunlight (by contrast to current emissive displays that are difficult to view in sunny conditions).[1,2] Black and white e-papers based on, for example, liquid crystal or electrophoretic displays, are already popular consumer products. However, it has been more challenging to develop high performance e-paper in color. In particular, image production based only on ambient light puts restrictions on maximum possible brightness. It is therefore not sufficient to only optimize color quality (chromaticity), but high-performance e-paper also requires high absolute reflection.[3] Recent research has explored various approaches to create highly reflective surfaces based on structural coloration of thin film cavities[4–9] or plasmonic[10–15] or dielectric metasurfaces.[16–18] These systems have further been combined with functional materials like liquid crystals, phase changing or electrochromic materials to switch such reflective surfaces on/off.[19–23] However, even if individual areas would provide 100% peak reflectance, creating color images using traditional RGB subpixels placed next to each other reduces the maximum reflectance to 33% at best, because each color can only occupy maximum one third of the total area. To circumvent this issue, we need to develop reflective pixels with tuneable colors (monopixels) instead of relying on neighboring pixels with fixed colors. Various approaches have been explored to dynamically tune the resonances and color of optical cavities and metasurfaces,[1,19,22,24–27] whereof some by electrical stimuli and to modulate reflected structural colors.[25,28,29] Among these are the use of materials with electrochromic properties to modulate nano-optical cavities and plasmonic devices.[3,30–32] As example, Peng et al. exploited the electrochemically tuneable refractive index (RI) of polyaniline to control the gap plasmons formed between polymer-coated plasmonic gold nanoparticles and a metal surface.[33] Color gamut and chromaticity are typically limited in such systems, partly due to limited RI-tuneability and the relatively absorptive nature of the electrochromic materials, respectively. Inorganic electrochromic materials like tungsten oxide (WO_3) have recently also been proposed for color tuning of optical cavities.[3,34,35] However, the tuning of any single WO_3 cavity structure did not cover the whole visible range,[3] mainly because the inorganic electrochromic materials did not provide sufficient RI variation and also did not change their thickness upon ion intercalation. To achieve full color tuning using a

S. Rossi, S. Chen, R. Shanker, D. Banerjee, M. P. Jonsson
Laboratory of Organic Electronics
Department of Science and Technology
Linköping University
Norrköping 60174, Sweden
E-mail: magnus.jonsson@liu.se
O. Olsson, A. Dahlin
Department of Chemistry and Chemical Engineering
Chalmers University of Technology
Gothenburg 41296, Sweden
The ORCID identification number(s) for the author(s) of this article can be found under https://doi.org/10.1002/adma.202105004.

DOI: 10.1002/adma.202105004

single cavity structure, it would be beneficial with an electroactive material that provides good actuation properties (also) in terms of thickness changes. It should preferably show only a small difference in absorption between its redox states (unlike WO_3) and operate at low voltages. As alternative optical systems, electrically responsive photonic crystals have shown promise for high wavelength tuneability,[36,37] although typically with limited brightness (≈20–30% peak reflectance) and relatively high operating voltages and switching speeds (several seconds). Electrophoretic tuning of photonic colloidal assemblies showed good time response,[38] but also with limited peak reflection (≈25%) and high operating voltages. Electrically tuneable soft-solid block copolymer structural colors based on stacking of two different dielectrics with ionic liquid reservoirs showed good tuneability,[39] yet not sufficient to cover the entire visible and requiring large applied voltages. Due to the easiness of fabrication and control of resonances, Fabry-Pérot (FP) cavities have been studied as a promising system for tuneable optical structural colors.[3,29,36,40,41]

In this paper, we present a dynamic reflective nano-optical cavity with high-chromaticity colors that can be reversibly tuned throughout the whole visible wavelength range and with high peak reflectance during tuning (50–60%). The novelty stems from the integration of a redox-tuneable conducting polymer as spacer layer of a hybrid nano-optical cavity, allowing for electrochemical modulation of the cavity resonance and reflected structural color using low operating voltages. Using in operando electrochemical microspectroscopy, we demonstrate reversible tuning of the cavity resonance by hundreds of nanometers in wavelength. We discuss the results in terms of thickness variations of the polymeric film upon electrochemical doping and dedoping, as well as variations in RI and the polymer's absorption coefficient. Importantly, the selected conducting polymer poly-thieno[3,4-b]thiophene (pT34bT) has a low bandgap and low visible absorption in both redox states,[42] thereby enabling the cavity to provide high and stable peak reflectance at 50–60% during the whole tuning cycle. Thanks to a reversed cavity design, the reflectance is further kept high by avoiding light to travel through the electrolyte and electrodes. In addition to continuous color tuning by gradual variation of the electrochemical potential, we demonstrate stepwise control of the color and the possibility to maintain the cavity resonance at different peak positions at will. The large tuning capability and overall results were consistent between different samples. To improve switching performance, we further implemented nanoholes in the cavity mirror to facilitate vertical electrolyte transport in and out of the electroactive polymer. We discuss remaining challenges, including the need for improving switching uniformity and long-term stability. Our work takes important steps toward tuneable monopixels for e-paper in color.

2. Results

2.1. Hybrid Polymer Nanocavities

Figure 1a illustrates the basic structure of the electroactive nano-optical cavity, formed by an electroactive thin polymer spacer sandwiched between an aluminum (Al, 50 nm) mirror and a semitransparent thin metal double layer of chromium (Cr, 5 nm) and gold (Au, 7 nm). We recently showed that optical cavities with such double metal top layer can provide high-quality reflection peaks via combined broadband absorber and FP effects.[4] In addition, the gold layer is conductive and enables the deposition of polymer thin films by oxidative electropolymerization (note the inverted cavity structure with the semitransparent layer on the substrate). Moreover, the gold layer is chemically inert, which helps to make the electrochemical switching stable. As electroactive spacer, we use the conducting polymer pT34bT (see chemical structure of the monomer in Figure 1a). Owing to its low bandgap,[43] pT34bT mainly absorbs in the near-IR range (see Figure S1a–c, Supporting Information), which makes it suitable as low-absorbing spacer for our nano-optical cavities. Simulations for pT34bT-filled cavities (Figure 1b,c(ii)) confirm the possibility to form hybrid cavities with a distinct reflection peak that is controllable from blue to red by increasing the spacer thickness (100–250 nm). The peak reflectance was highest (51%) for 105 nm spacer thickness (405 nm peak wavelength) and reduced to 34% for devices with 250 nm thick spacers (690 nm peak wavelength) (Figure 1b). The lower reflectance at longer wavelengths is due to thicker spacer combined with increasing imaginary refractive index toward the red region for the pristine oxidized state of the polymer (Figure S1a, Supporting Information).

We experimentally fabricated the same type of pT34bT-filled cavities by electropolymerization on chromium and gold-coated glass substrates followed by thermal evaporation of aluminum. The electrodeposited layer was dense and with a low surface roughness (Figure S1d–f, Supporting Information). Varying the polymer thickness led to cavities with resonances spanning the whole visible spectrum (Figure 1c,d). The cavities provide high-quality reflection peaks, resulting in vibrant structural colors, including violet, blue, green, yellow, orange, and red. As clear from Figure 1c, we found good agreement of the reflectance peak and dip positions between simulated and experimental results. In accordance with the simulations, the peak reflectance is high (>50%) for the thin cavities and it decreases with the increase of spacer thickness to ≈35% for the thickest cavity. The thickest cavities (216 and 271 nm) also present a second order peak appearing in the blue region (see Figure S4 of the Supporting Information for simulations of even thicker cavities and their higher orders). We note that the experimental results present overall higher reflectance than the simulations. This is in part due to experimental normalization to an aluminum mirror (with absolute reflectance from ≈92.4% to 89.5% in the visible, see Figure S13c, Supporting Information) and in part due to broadband reflection at the glass/air interface at the backside of the substrate (4–5%), which the simulations do not account for. The resulting higher baseline reflection increases the overall reflectance for the fabricated cavities, but at the same time, it lowers the chromaticity compared to the simulated results. This suggests that the color gamut may be further improved by the implementation of antireflection coatings.

2.2. Dynamic Modulation of Electroactive Polymer Nanocavities

After verifying that pT34bT-filled nano-optical cavities can provide vibrant structural colors, we investigate the possibility

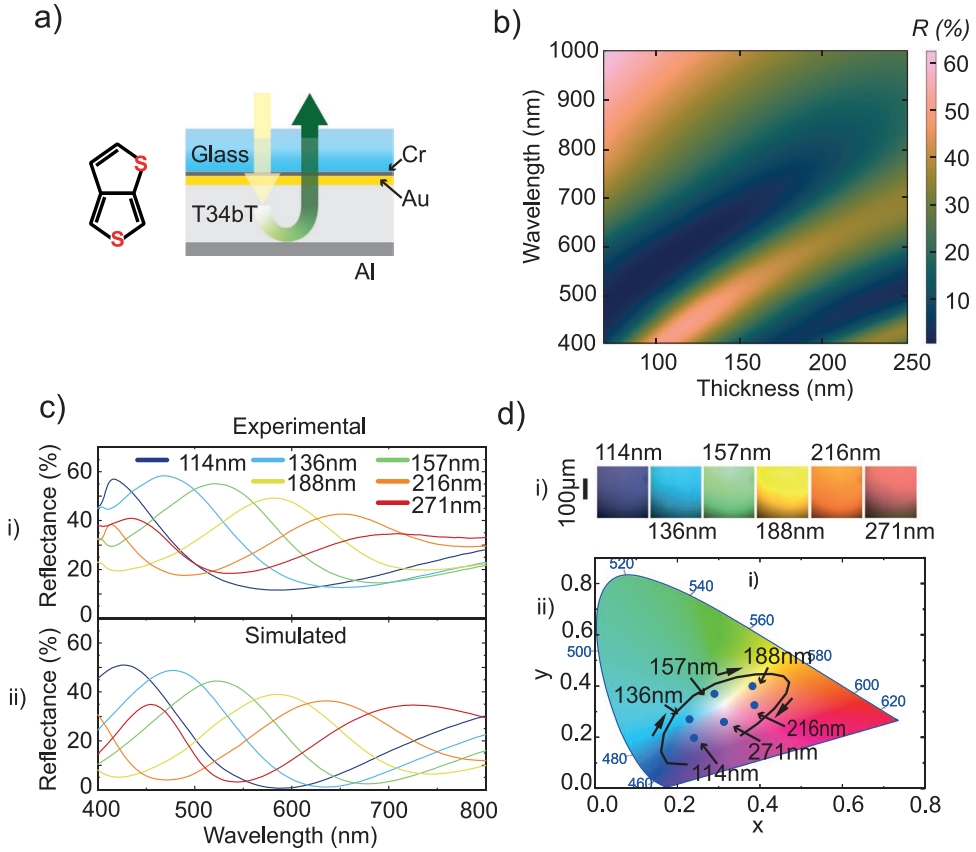

Figure 1. Optical properties of static pT34bT-filled optical cavities of different thicknesses. a) Molecular structure of T34bT and schematic illustration of the polymer-filled nano-optical cavities. b) Reflectance color map for simulated reverse optical cavities (with 5 nm Cr and 7 nm Au as the semi-transparent mirror) for different thicknesses of the pT34bT spacer. c) Experimental (i) and simulated (ii) reflectance spectra of pT34bT-filled optical cavities with different polymer thicknesses. d) (i) Microscope images (50× magnification) of the same cavities as presented in (c). (ii) CIE diagram corresponding to the experimental data in (c) (blue points) and the simulated data in (b) (solid line).

to tune their properties by electrochemical modulation of the polymer redox state. **Figure 2**a illustrates the measurement procedure, based on an electrochemical fluidic cell positioned under a microscope capable of recording reflection spectra from ≈15 µm in diameter circular spots (see the Experimental Section for details). To allow electrochemical switching, we patterned the top aluminum mirror into pixelated areas (0.2 × 0.2 to 0.8 × 0.8 mm^2). This ensured contact between the polymer and the electrolyte (0.1 M sodium dodecylbenzenesulfonate [NaDBS] in water) at the sides of each pixel. The active area of the working electrode in the cell was 1.33 cm^2. While not the optimum configuration in terms of electrolyte transport in and out of the polymer, these pixels could switch remarkably well (typically after several precycles) and they thereby provide a suitable cavity system for investigation of variations in optical properties during switching. We emphasize that the unconventional inverse cavity design allowed inspection of the cavity samples from their backside, without need to image through the electrolyte or any electronics (see right part of Figure 2a). In this way, the reflectance can remain high also for switching measurements and complete devices, as we recently demonstrated for hybrid inorganic nano-optical cavities.[3] In turn, this forms a key factor for future reflective displays in color.

Figure 2b shows switching results for a cavity with an initial polymer thickness of ≈106 nm. We modulated the electrochemical potential in a cyclic manner between −1 and +0.7 V at 50 mV s^{-1} and present data after stabilization with 38 cycles (Figure 2b–d, see Figure S6a,b for cyclic voltammetry (CV) and charge evolution over many cycles). Figure 2b(i) shows the corresponding variation of the cavity reflectance as a color map over time for a small area on a pixel, with peak position indicated as the black solid line. Excitingly, switching the optical cavity led to large blue-shifts in oxidation and red-shifts in reduction. The cavity resonance reversibly shifted by more than 230 nm, all the way from the blue region (reflectance peak position at 454 nm) to the red (peak position at 695 nm). The results suggest that the pT34bT film shrinks in oxidation and expands in reduction, as reported in terms of mass change for the same polymer with polystyrenesulfonate as counter ion.[43] Under the assumption that the RI does not change during switching (using data from Figure S1, Supporting Information), this corresponds to a thickness change of more than 100%. If we instead assume that the observed cavity tuning would be due only to variation in the polymer's real RI, it would have to increase by as much as 1.4 upon reduction to shift the cavity resonance from blue to red, which we believe is not plausible (see Figure S5a,b, Supporting Information). Ellipsometry

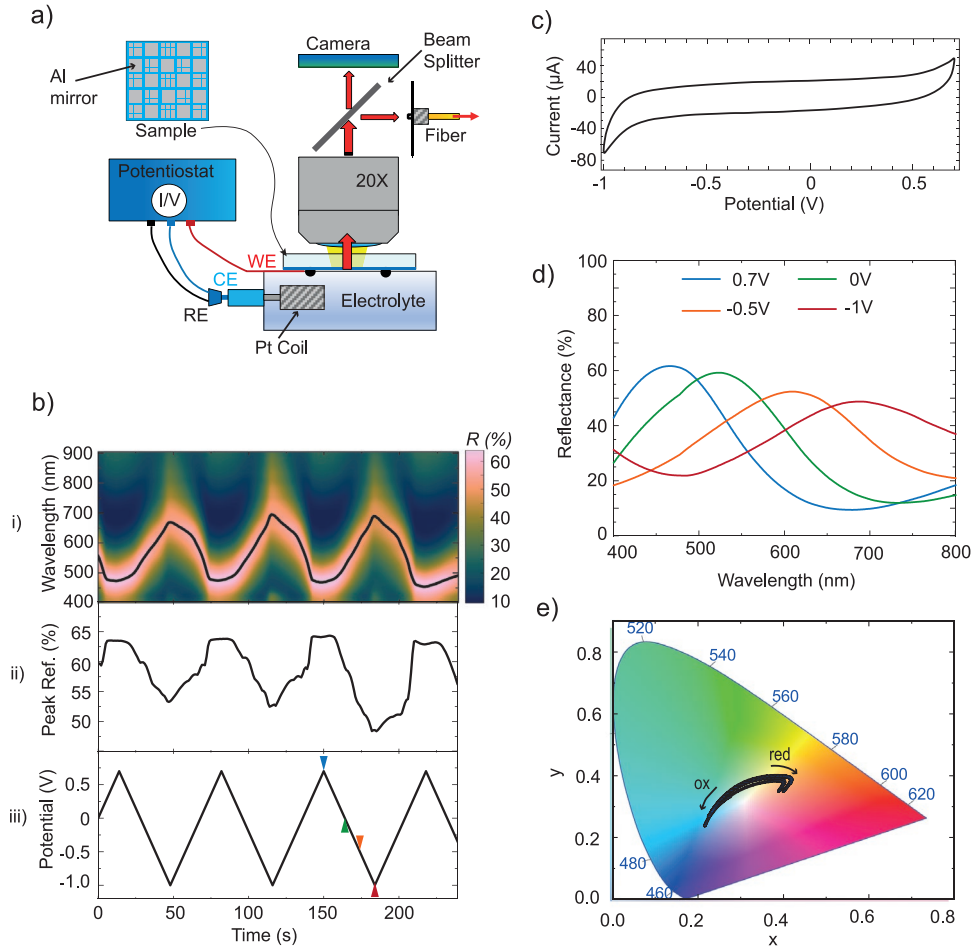

Figure 2. Dynamic modulation of pT34bT-filled optical cavities. a) Schematic illustration of the microspectroscopic measurements. b) Temporal variation of the cavity during several cyclic voltammetry cycles, showing: (i) experimental reflectance color map (with the peak position marked as the solid line), (ii) peak reflectance, (iii) applied potential. c) Experimental results for one CV cycle (after 38 stabilizing pre-cycles). d) Selected reflectance spectra at different potentials (from the third cycle, see markings in (b iii)) for different potentials. e) CIE diagram obtained from the tuneable cavity reflectance (from (d)).

measurements of chemically reduced pT34bT samples in air (see Figure S3a,b and details in the Supporting Information) revealed an increase in RI compared to the original (p-doped, as electropolymerized) state. Such increase in RI may contribute to the red-shift of the cavity resonance but is far from enough to explain the full color tuneability of the cavities (Figure S3c, Supporting Information). Complementary surface plasmon resonance (SPR) measurements of electropolymerized pT34bT films on gold showed an increase of the SPR angle upon reduction (Figure S16a,b, Supporting Information). This is compatible with refractive index (and/or thickness) increase, but the shifts were too small to explain any major changes in refractive index during switching. Assuming that the thickness would not change during the switching, the SPR shift would correspond to an RI change on the order of 0.1 (Figure S16c, Supporting Information), which is one order of magnitude lower than the one required to explain the tuning range of the electroactive cavities. This indicates that thickness variations are involved in the tuning process. On the other hand, only swelling the film by dilution (of its optical properties) would lead to the opposite SPR response, indicating that the reduction must also be associated with changes to the polymer's optical properties.[44] Polymer thickness monitoring during switching by electrochemical quartz crystal microbalance (QCM) measurements confirmed that the polymer shrinks in oxidation and swells in reduction (Figure S17, Supporting Information), although to a lower extent than that required to on its own explain the large cavity tuning. The lower thickness variation may be related to that the QCM (and SPR) measurements relate to the average response for large pT34bT thin films while the microspectroscopy measurements are local. In turn, we found that not all cavity pixels switched and also that there were often variations even within single pixels (e.g., see Figures S11 and S15c, Supporting Information). From the combined results we conclude that the cavity tuning most likely involves significant thickness variations, possibly aided by changes in RI as discussed further below. Indeed, conducting polymers have previously shown the capability of providing redox-tuneable thickness or volume variations, which forms an important difference from inorganic electrochromic materials when implemented into cavities.[3,30] For example, polypyrrole cycled in a similar electrolyte (NaDBS in water) was reported to change its thickness by ≈60–100%

upon the first cycle and 30–40% between the oxidized and reduced state for the following cycles.[45] Poly(3,4-propylenedioxythiophene (PProDOT) was shown to change volume by up to 30% when varying its redox state, also accompanied with alteration of its elastic modulus and softness by a factor of two.[46] Another thiophene-based polymer recently showed an impressive 300% reversible expansion via solid-gel switching.[47] Thickness variations for our electroactive cavities are likely related to Na^+ ions being expelled from the polymer in oxidation to compensate for the gained positive charge, while there is an uptake in reduction to compensate for the loss of positive charge. In that respect, we note that the electrolyte composition is important for the thickness variations. For example, previous reports using 0.1 M lithium trifluoromethanesulfonate in ACN/nitrobenzene showed even opposite behavior for pT34bT, with a small loss in film mass upon reduction due to transport of anions out of the polymer.[48] For our system, the mass/thickness change instead seems to be largely related to cation transport, likely due to the bulky size and low mobility of the anion. Changing the electrolyte to 0.1 M a Na_2SO_4 solution in water led to considerably lower peak variations (see Figure S7, Supporting Information).

As shown in Figure 2b(ii), the peak reflectance remained high when electrochemically reducing the polymer and tuning the cavity resonance from the blue/cyan (63% at 470 nm) to the red (53% at 690 nm). We observed only a small decrease in peak reflectance when electrochemically red-shifting the cavity resonance, and much smaller than for the static cavities of different polymer thicknesses (compare Figure 1c(i) with spectra for the dynamically tuned cavity in Figure 2d). Hence, electrochemical modulation allows us to obtain cavities that can be tuned throughout the whole visible range with stable peak reflectance, which is promising for use as monopixels in reflective displays.

The maintained high reflectance for the reduced red-shifted cavity implies that the polymer does not only swell but also undergoes favorable changes in its optical properties upon reduction. Indeed, transmittance measurements for thin polymer films on semitransparent metal layers showed that the polymer film becomes only slightly more absorptive in the red upon reduction (Figure S2a, Supporting Information) and less than expected if the tuning would arise only from increasing the polymer thickness without changing its permittivity (see comparison in Figure S2b, Supporting Information). A possible explanation is that electrochemical reduction swells the polymer by water uptake and that this leads to reduced absorption coefficient and thereby only a moderate increase in total absorption. Furthermore, the results may be related to that the cavity-tuning is aided by an increase in polymer RI upon reduction, which reduces the film thickness required to red-shift the cavity resonance to a given position. We recently discovered a similar synergistic control of permittivity and thickness when exploring structural colors in UV-controlled vapor phase polymerized poly(3,4-ethylenedioxythiophene) thin films on metals.[40]

In Figure 2e, we have converted the reflectance spectra from cavity switching to coordinates in a CIE diagram, again confirming that the electroactive cavity could be tuned throughout the visible region. The oxidized cavity shows blue reflection, which is gradually tuned to cyan, green, orange, and red upon reduction. The chromaticity is somewhat limited for green color, partly attributed to modest peak quality factor and comparably high background reflection. When increasing the reduction into the red region of the CIE diagram, the graph turns due to the appearance of a second-order peak in the blue, as visible also in Figure 2b(i) and discussed in relation to Figure 1. The results in Figure 2 indicate that the electrochemical cavity tuning is reversible and reproducible. For more extensive cycling (on the order of tens to hundreds of cycles), we often observed permanent shifts in resonance positions for both states of the polymer (Figure S8a, Supporting Information). Such effects may, for example, be reduced by carefully adjusting the electrochemical window during modulation and monitoring the charge variation to avoid overoxidation.

2.3. Stepwise Electrochemical Control of Cavity Resonances

For practical applications, it is important to be able not only to continuously tune the cavity resonance, but to also stop at selected colors. To investigate this ability, we monitored the reflectance for an electroactive cavity while stepwise changing the electrochemical potential to different predefined values. As shown in **Figure 3**a(i), the reflectance peak position largely followed the voltage variations (Figure 3a(iii)), although the position did not always come back to exactly the same value for the same voltage. An example of more chronoamperometry cycles is presented in Figure S9a of the Supporting Information for a similar sample, showing 10 cycles with stable performance. Notably, the sample presented in Figure 3 showed a very large wavelength tuning range of 365 nm (from peak position at 472 nm at +0.8 V to 837 nm at −1.0 V). This tuning range is larger than that presented in Figure 2 for CV tuning, as attributed primarily to the voltage being varied continuously during CV and thereby not allowing the sample to reach its full tuning range due to limited ion transport under the mirror. Indeed, this agrees with our findings of reduced tuning range at higher CV sweep speeds (Figure S8b–d, Supporting Information) and with the relatively slow peak shifting in chronoamperometry (Figure S9b, Supporting Information). In agreement with the results for CV tuning, the magnitude of the peak reflectance maintained high also upon stepwise switching (Figure 3a(ii)), with only very small variations in the range between 57% and 63% even when red-shifting the peak position beyond 800 nm. As clear from the CIE diagram (Figure 3b), it was also possible to maintain good chromaticity in the entire visible range. This behavior is also clear from microscope images obtained of the sample at each potential step (Figure 3c). The reason why the cavity first shifts from blue toward red upon reduction but then back again toward blue for yet larger reduction voltages is that the primary resonance moves even into the near-infrared range and a second-order peak appears in the blue. We often observed gradual variation in color from the sides of the pixels, in agreement with ion diffusion toward the inner part of the pixels taking a considerable amount of time for these relatively large cavities (0.2×0.2 mm^2 and 0.8×0.8 mm^2 for small and big pixels, respectively). In the particular example shown in Figure 3c, this same effect also appeared within the pixel, which may be due to crack formation that presumably opens access for electrolyte transport. Despite microscopic

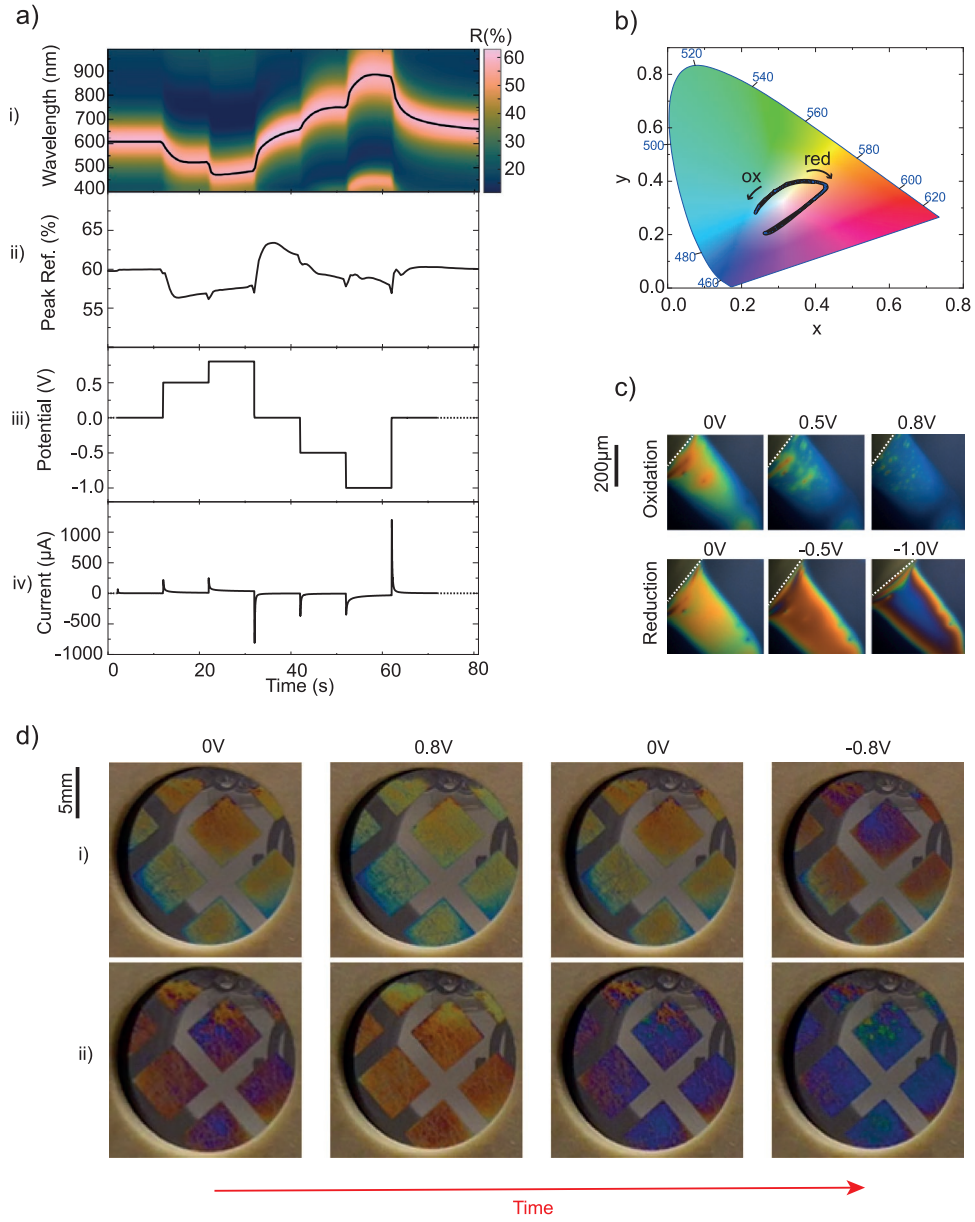

Figure 3. Stepwise color tuning of electroactive optical cavities. a) Experimental results for stepwise tuning by chronoamperometry for a sample with 5×5 mm^2 pixels, showing (i) reflectance color map and peak position (solid line) versus time, (ii) peak reflectance over time, (iii) applied potential, and (iv) the corresponding measured current (for 1.33 cm^2 electrode area). b) CIE diagram obtained from conversion of the reflectance spectra in (i). c) Microscope images collected at different voltage steps, as indicated in the panel. The white dotted line indicates the mirror and Al mirror edge. d) Large-scale photographs of the electrochemical cell containing a cavity sample with 5×5 mm^2 pixels while performing chronoamperometry (three-electrode configuration) after (i) 15 and (ii) 20 chronoamperometry cycles (after 30 pre-CV cycles), in the sequence indicated by the time arrow.

inhomogeneities, we found that the pT34bT-filled cavities could produce tuneable colors also at the macroscale. This is exemplified in Figure 3d and Movie S1 of the Supporting Information for large (5×5 mm^2) pixels controlled by chronoamperometry. While the previous results demonstrated successful two-electrode switching, as essential for practical devices, these measurements were performed using a 3-electrode configuration (see the Experimental Section for details). Figure 3d shows photographs of a pT34bT-filled nanocavity sample with 5×5 mm^2 pixels during chronoamperometry switching from 0 to 0.8 V, back to 0 V, and finally reduced to –0.8 V. We note that the switching seems to involve the full areas of these large pixels, which is rather remarkable considering that there is an Al mirror layer on top of the polymer. This may be due to unintended openings in the Al mirror, possibly formed during redox cycling of the polymer and strain induced during swelling and deswelling. Microscopic investigation by SEM indeed revealed some cracks and openings, in particular for samples that were switched many cycles (>100, Figure S15, Supporting Information). On a larger scale, we noticed variations in color

due to geometrical factors of the electrochemical cell, with the switching starting preferentially on the area closer to the counter and reference electrodes inside the fluidic cell. The pixel colors could be reversibly controlled on short time scales, while we observed permanent red-shifts of the spectral features for larger number of switching cycles (both in chronoamperometry and CV). This is clear from the difference between results for the 15th chronoamperometry cycle (Figure 3d(i)) and the 30th cycle (Figure 3d(ii), after an initial 30 CV repetitions). Continued cycling by CV (measured for a different sample) could also lead to evolution of the microscale color variations (Figure S11, Supporting Information).

2.4. Nanohole-Assisted Electroactive Optical Cavities

To intentionally allow vertical electrolyte transport, we fabricated devices with nanoholes in the Al layer facing the electrolyte (see schematic in **Figure 4**a). Similar strategies have been successful for inorganic hybrid nanocavities and systems filled with polymers that change thickness upon heat stimuli.[3,49] We formed ≈200 nm in diameter nanoholes in the 50 nm thick Al mirror by colloidal lithography,[50] resulting in well-dispersed short-range ordered distribution over the surface (see scanning electron microscopy image in Figure 4b). The nanoholes did not significantly modify the cavity resonance in the visible (Figure S13a, Supporting Information) except for decreased overall reflectance due to lower reflectivity of the mirror (Figure S13b, Supporting Information). The nanohole-assisted cavities started switching after only ≈10–20 cycles and provided widespread switching across the sample. Interestingly, the investigated nanohole cavity samples provided extremely large reversible wavelength tuning of ≈430 nm (upon CV in a two-electrode setup at 50 mV s^{-1}, see Figure 4c,d). Remarkably, this large wavelength tuning was again accompanied by maintained high peak reflectance during tuning (Figure 4d(ii)). Furthermore, the exceptional tuning enabled the second order resonance peak to red-shift beyond 450 nm (Figure 4d(i)), which resulted in a blue color with good chromaticity (see CIE diagram in Figure 4c). By contrast to the standard cavities without nanoholes in the top mirror, the nanohole-assisted cavities could provide large tuning range also at high CV sweep speeds, with shifts in peak position of ≈290 nm at 200 mV s^{-1} (Figure 4e). This shows that the nanoholes aid the switching process. Furthermore, nanohole-assisted cavity devices could provide reversible tuning over more than 40 chronoamperometry cycles (Figure S10, Supporting Information). On the other hand, we found that adding nanoholes to the Al mirror did not remove microscale inhomogeneity of the cavity colors upon switching, and nonhomogeneous effects could even be observed where there was no metal between the electrolyte and the polymer (see Figure S12, Supporting Information).

The nanohole cavity samples presented in Figure 4 were still designed as pixels. To avoid the possibility for the electrolyte to enter through pixel sides, we also prepared samples composed of only one single large cavity. Interestingly, these systems showed modified tuning behavior, with red-shifted resonances for both large oxidation and reduction potentials and lower wavelength resonances for intermediate potentials (Figure S14a–c, Supporting Information). In this respect, we note that a partial red shift at high oxidation (0.8 V) was also present for the pixelated samples with nanoholes (Figure 4d(i)), although this effect was much smaller than for the nonpixelated nanohole cavities. A possible reason may be related to the formation of localized strain patterns that were seen for those samples (see Figure S14c, Supporting Information) and not for the other types. While the fully covered nanoholes samples could still provide large peak shifts, the switching was less controllable compared with pixelated samples, with more rapid degradation and drifts upon multiple cycles.

3. Conclusions

Our study shows that integrating electroactive conducting polymers into optical nanocavities enable reversible color tuning across the entire visible range and beyond with maintained high peak reflectance during tuning. Our results suggest that switching involves large polymer thickness variations, combined with favorable low visible absorption for the chosen polymer and possibly aided by synergistic RI changes. Implementing nanoholes in the Al mirror facing the electrolyte could further improve switching performance and provide tuning of the reflectance peak by more than 400 nm, still with maintained high peak reflectance during tuning. Future work will preferably address remaining challenges such as long-term stability and improvement of uniformity, for example, by exploring alternative polymers, and strategies for improved polymer–metal adhesion. We further suggest that reduction of pixel size to micrometric dimensions (e.g., in the implementation with a TFT array) may be favorable to improve homogeneity and switching speeds, by reducing ion diffusion lengths and avoiding electrochemical breathing modes in the entire sample.[46]

Importantly, the large tuning range of our electroactive cavities greatly supersedes that of recently reported cavities comprising inorganic electrochromic spacer layers.[3,30,36] The tuning range is also larger than that reported for cavities actuated by electrostriction or ion liquid swollen block copolymers, yet with orders of magnitude lower operating lower voltages than the first[51,52] and smaller electrochemical window than the latter.[39] Electroactive inverse opals showed impressive tuning capability, yet with limited peak reflectance and ≈2–3 times higher operating voltages than used in this work.[34] By covering the whole visible at low operating voltages and with maintained high peak reflectance during tuning, our concept takes important steps toward tuneable monopixels for e-paper in color, without having to adopt subpixel division and thereby avoiding corresponding losses in brightness. In turn, high brightness is critical for reflective displays because they are limited to producing images using ambient illumination. The inverse cavity design is particularly appealing in this respect as it allows viewing of the cavities from the backside of the device and thereby further avoids a reduction in reflectance from light passing through the electrolyte and electronics. The use of conducting polymers could also open for flexible devices, with switching based on gel electrolytes.[53] Finally, we note that the

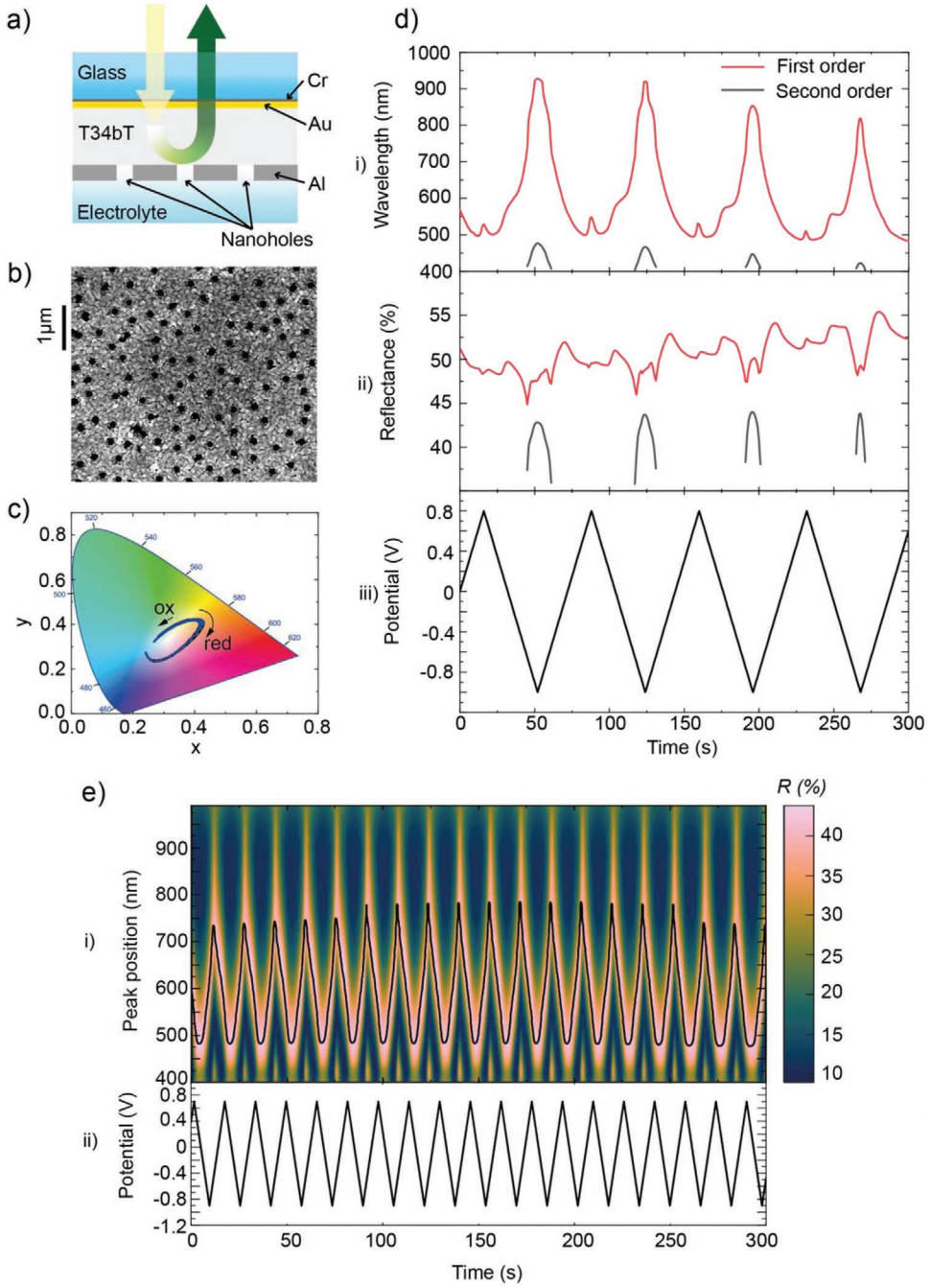

Figure 4. Dynamic tuning of nanohole-assisted polymer-filled cavities. Sample with ≈200 nm diameter nanoholes in the top patterned Al mirror. a) Schematic illustration of the nanohole-based cavities. b) Scanning electron microscopy image of a cavity with the Al mirror perforated with nanoholes. c) Microspectroscopy switching results upon cyclic voltammetry (two-electrode configuration) showing the time evolution of (i) the peak position, (ii) the peak reflectance for the first (red line) and second (black line) order resonances, and (iii) applied voltage. d) CIE diagram corresponding to the same tuning cycles as in (c). e) Tuning results for CV at 200 mV s^{-1} for another nanohole-assisted cavity, showing (i) reflectance color map (with identified peak position marked by the black curve), and (ii) applied voltage.

presented concept to place functional polymers inside optical nanocavities may be used for other applications as well as to study the polymers themselves, for example, using color variations to extract information about spatial and temporal polymer thickness variations. The suggested high thickness changes of pT34bT, along with its reversibility and expansion control by voltage, might also be used in the field of actuators. In addition, the polymer may be a suitable candidate for other types of tuneable photonic systems, such as metasurfaces and photonic crystals. Further studies are necessary to determine the exact swelling capabilities of pT34bT and the relation with its structural changes between the oxidized and reduced states.

4. Experimental Section

Optical Cavity Preparation: The substrates were made from 18 × 18 mm slide glass size 2 (Corning) that were ultrasonicated in 2% soap solution (Hellmanex) in deionized water, deionized water, acetone, isopropyl alcohol (IPA), and then rinsed in IPA and cleaned by UV-ozone for 30 min. The substrates were then coated with 5 nm Cr and 7 nm Au at a rate of 2 Å s^{-1} by thermal evaporation (PVD handy 2T, Vaksis). They were then cleaned by 15 min UV-ozone treatment before further processing.

Thieno[3,4-b]thiophene (pT34bT, Accela ChemBio Inc.) was diluted in acetonitrile in a mother solution and the concentration of the monomer was then determined by UV–vis. pT34bT was then diluted with a 0.01 M concentration in a 0.1 M Sodium dodecylbenzenesulfonate (NaDBS, Sigma-Aldrich) deionized water solution, used as the electrolyte. To dilute the pT34bT mother solution, it had first to be dried from acetonitrile using a nitrogen stream, then ultrasonicated for 15 min and stirred for ≈2 h in its electrolyte.

The electropolymerization was done using chronoamperometry at a fixed potential of 700 mV versus an Ag/AgCl reference (RE1-B, Biologic) with a potentiostat (Biologic, SP-200) and a Pt-gauze (A-002250, Biologic) as the counter electrode. The substrate was dipped directly in a beaker with the monomer/electrolyte solution. The thickness was controlled by controlling the amount of deposited charge. Unless otherwise stated, all the samples were electropolymerized with a deposited charge per area from 9 to 13 mC cm^{-2} deposited charge corresponding to a thickness from 106 to 114 nm. The samples were then rinsed in deionized water and dried with a nitrogen gun. The top Al mirror was evaporated using a shadow mask with a rate of 15 Å s^{-1} and a thickness of 50 nm, to obtain a patterning of the optical cavity. The shadow mask was designed with clusters of square pixel sizes of 0.2 × 0.2 mm^2 and 0.8 mm × 0.8 mm^2.

Nanohole Fabrication: Nanoholes were fabricated by colloidal lithography using 197 nm diameter polystyrene (PS) nanoparticle (from Microparticles GmbH) suspended in a 0.1% weight solution in deionized water. After cleaning (rinsed in deionized water and dried with a nitrogen gun), the samples were treated by a 2% weight solution of polydiallyldimethylammonium chloride in water (polyDDA, 522376, Sigma-Aldrich) for 60 s to positively charge the surface and then rinsed for 40 s in deionized water. Then the samples were left for 60 s in the PS solution and rinsed with deionized water for 40 s. The evaporation of the top Al mirror was done as for the substrate. After the evaporation, the PS nanoparticles were removed by peeling them off with tape.

Spectroelectrochemical Characterization: The spectroelectrochemical characterization was done using a custom-made electrochemical cell (Back microscopy EFC, Redox.me) in a 2-electrode configuration, connected to a potentiostat (SP-200, Biologic, and Autolab PGSTAT204, Metrohm). A 0.6 mm diameter and 250 mm long wire platinum coil in helix was used as the counter electrode. The exposed area of the sample to the electrolyte, corresponding to the working electrode area, was 1.33 cm^2. NaDBS 0.1 M was used in deionized water as the electrolyte, as done for the electropolymerization. Both cyclic voltammetry and chronoamperometry were used to characterize the spectral response. The cell was placed in a microscope (Nikon Eclipse L2000N) with a 20× objective connected to a spectrophotometer (QePRO, OceanOptics) with a 50 µm diameter optical fiber (Thorlabs, M14L05). The integration time was set to 100 ms. The use of a small diameter fiber ensured to collect the signal from a limited circular spot of ≈15 µm diameter in the focal plane. The microscope was equipped with a beam splitter (ThorLabs, SM1CP2) to direct part of the beam into a camera (Infinity 1, Lumenera) having the same focal plane of the output fiber order to be able to simultaneously take pictures and spectra of the sample. All the reflectance data were normalized to an Al mirror, evaporated on a glass substrate at the same rate and thickness of the optical cavities top mirror. A smoothing function ("loess" in Matlab, a local regression using weighted linear least squares and a 2nd-degree polynomial mode) was applied to the spectra to eliminate noise when collecting with a 50 µm fiber.

Optical and Thickness Characterization: The optical properties of the electropolymerized film were determined by ellipsometry (RC2, J.A. Woollam), depositing the polymer in a Si-wafer coated with 5 nm of Cr and 70 nm of gold to have a highly flat surface as the reference. The data were fitted to get both the thickness and the refractive index of the polymer. The thickness of the electropolymerized film was measured by a thin film analyzer (Filmetrics) with a fiber probe, using the ellipsometric data as the refractive index. In the fitting, the refractive indexes and all the thicknesses of the other layers were kept constant except the thickness of the pT34bT, which was the only fitting parameter.

Surface Plasmon Resonance Measurements: The SPR measurements were made in a BioNavis SPR Navis 200A with an electrochemical cell with a three-electrode setup. The counter electrode was a Pt-wire and the reference electrode were Ag/AgCl adjusted to a commercial Ag/AgCl electrode. PT34bT:DBS were polymerized upon the sensors (2 nm Cr and 50 nm Au, BioNavis) in a separate electrochemical cell and then used as working electrode in the SPR. Pulses of 30 s were used to switch the polymer. The reference spectra were made by removing the polymer and repeating the experiment. All measurements were made with stagnant electrolyte.

Possible states for RI and the height of the polymer were found by simulations of the SPR-spectra (MATLAB). The reference (no polymer) was first fitted by varying the RI of the SPR-system for a fixed thickness. No perfect fits could be found (R^2 around 0.8) but we focused on fitting the SPR angle and the width of the peak. An offset of the simulated spectra was used to superimpose the simulated SPR-dip to the experimental.

E-QCDM: The E-QCMD measurements were performed in an electrochemical cell w Q-SENSE D4 with an electrochemical module, Pt-counter and Ag/AgCl reference (WPI). The sensors were Au/Cr 5 MHz (Quartz Pro). The electrochemical experiments (cyclic voltammetry) were made in a 0.1 M NaDBS electrolyte and the polymerization of PT34bT:DBS onto the sensors was done inside the cell. Electrochemical switching experiments were done in monomer-free electrolyte before and after polymerization.

Simulations: The optical response was simulated of cavity systems using Comsol Multiphysics with the Wave Optics module, using a p-polarized plane wave as the source with normal incidence. A 2D periodic model with a period of 300 nm and a symmetric mesh with a maximum size of 40 nm was used. The refractive index data for T34bT were taken from the experimental ellipsometric determination.

Supporting Information

Supporting Information is available from the Wiley Online Library or from the author.

Acknowledgements

This work was funded by the Swedish Foundation for Strategic Research. Additional support was provided by the Knut and Alice Wallenberg Foundation, the Swedish Research Council (VR), the Wenner-Gren Foundations, and the Swedish Government Strategic Research Area in Materials Science on Functional Materials at Linköping University (Faculty Grant SFO-Mat-LiU No. 2009 00971).

Conflict of Interest

The authors declare no conflict of interest.

Data Availability Statement

The data that support the findings of this study are available from the corresponding author upon reasonable request.

Keywords

color-tuning, conductive polymer, electroactive nanocavity, reflective displays, structural colors

Received: June 30, 2021
Revised: August 20, 2021
Published online:

[1] K. Xiong, D. Tordera, M. P. Jonsson, A. B. Dahlin, *Rep. Prog. Phys.* **2019**, *82*, 024501.
[2] D. Y. Kim, M. J. Kim, G. Sung, J. Y. Sun, *Nano Convergence* **2019**, *6*, 21.
[3] M. Gugole, O. Olsson, S. Rossi, M. P. Jonsson, A. Dahlin, *Nano Lett.* **2021**, *21*, 4343.
[4] S. Rossi, M. P. Jonsson, *J. Opt.* **2021**, *23*, 015001.
[5] C. Ji, S. Acharya, K. Yamada, S. Maldonado, L. J. Guo, *ACS Appl. Mater. Interfaces* **2019**, *11*, 29065.
[6] C. Yang, W. Shen, J. Zhou, X. Fang, D. Zhao, X. Zhang, C. Ji, B. Fang, Y. Zhang, X. Liu, L. J. Guo, *Adv. Opt. Mater.* **2016**, *4*, 1981.
[7] S. Sardar, P. Wojcik, E. S. H. Kang, R. Shanker, M. P. Jonsson, *J. Mater. Chem. C* **2019**, *7*, 8698.
[8] T. Guo, J. Evans, N. Wang, S. He, *Opt. Express* **2019**, *27*, 21646.
[9] A. M. Shaltout, J. Kim, A. Boltasseva, V. M. Shalaev, A. V. Kildishev, *Nat. Commun.* **2018**, *9*, 2673.
[10] L. Wang, R. J. H. Ng, S. Safari Dinachali, M. Jalali, Y. Yu, J. K. W. Yang, *ACS Photonics* **2016**, *3*, 627.
[11] H. Wang, X. Wang, C. Yan, H. Zhao, J. Zhang, C. Santschi, O. J. F. Martin, *ACS Nano* **2017**, *11*, 4419.
[12] A. Kristensen, J. K. W. Yang, S. I. Bozhevolnyi, S. Link, P. Nordlander, N. J. Halas, N. A. Mortensen, *Nat. Rev. Mater.* **2016**, *2*, 16088.
[13] F. Ding, Y. Yang, R. A. Deshpande, S. I. Bozhevolnyi, *Nanophotonics* **2018**, *7*, 1129.
[14] X. M. Goh, R. J. H. Ng, S. Wang, S. J. Tan, J. K. W. Yang, *ACS Photonics* **2016**, *3*, 1000.
[15] A. S. Roberts, A. Pors, O. Albrektsen, S. I. Bozhevolnyi, *Nano Lett.* **2014**, *14*, 783.
[16] K. Baek, Y. Kim, S. Mohd-Noor, J. K. Hyun, *ACS Appl. Mater. Interfaces* **2020**, *12*, 5300.
[17] R. Shanker, S. Sardar, S. Chen, S. Gamage, S. Rossi, M. P. Jonsson, *Nano Lett.* **2020**, *20*, 7243.
[18] H. Nishi, T. Tatsuma, *ACS Appl. Nano Mater.* **2019**, *2*, 5071.
[19] D. Franklin, R. Frank, S. T. Wu, D. Chanda, *Nat. Commun.* **2017**, *8*, 15209.
[20] K. Xiong, D. Tordera, G. Emilsson, O. Olsson, U. Linderhed, M. P. Jonsson, A. B. Dahlin, *Nano Lett.* **2017**, *17*, 7033.
[21] T. Xu, E. C. Walter, A. Agrawal, C. Bohn, J. Velmurugan, W. Zhu, H. J. Lezec, A. A. Talin, *Nat. Commun.* **2016**, *7*, 10479.
[22] F. Liu, H. Shi, X. Zhu, P. Dai, Z. Lin, Y. Long, Z. Xie, Y. Zhou, H. Duan, *Appl. Opt.* **2018**, *57*, 9040.
[23] K. Xiong, G. Emilsson, A. Maziz, X. Yang, L. Shao, E. W. H. Jager, A. B. Dahlin, *Adv. Mater.* **2016**, *28*, 10103.
[24] S. Chen, E. S. H. Kang, M. Shiran Chaharsoughi, V. Stanishev, P. Kühne, H. Sun, C. Wang, M. Fahlman, S. Fabiano, V. Darakchieva, M. P. Jonsson, *Nat. Nanotechnol.* **2020**, *15*, 35.
[25] E. K. Chan, T. Chang, T. C. Fung, J. Hong, C. Kim, J. Ma, Y. Pan, S. G. Wang, B. Wen, *J. Microelectromech. Syst.* **2017**, *26*, 143.
[26] G. Wang, X. Chen, S. Liu, C. Wong, S. Chu, *ACS Nano* **2016**, *10*, 1788.
[27] E. Balaur, C. Sadatnajafi, S. S. Kou, J. Lin, B. Abbey, *Sci. Rep.* **2016**, *6*, 28062.
[28] S. Zhang, S. Yu, J. Zhou, J. F. Ponder, M. J. Smith, J. R. Reynolds, V. V. Tsukruk, *J. Mater. Chem. C* **2019**, *7*, 3090.
[29] C. Sung, J. Han, J. Song, C. S. Ah, S. M. Cho, T. Y. Kim, *Adv. Mater. Technol.* **2020**, *5*, 2000367.
[30] Z. Wang, X. Wang, S. Cong, J. Chen, H. Sun, Z. Chen, G. Song, F. Geng, Q. Chen, Z. Zhao, *Nat. Commun.* **2020**, *11*, 302.
[31] E. Hopmann, A. Y. Elezzabi, *Nano Lett.* **2020**, *20*, 1876.
[32] Y. Li, J. Van De Groep, A. A. Talin, M. L. Brongersma, *Nano Lett.* **2019**, *19*, 7988.
[33] J. Peng, H. Jeong, Q. Lin, S. Cormier, H. Liang, M. F. L. De Volder, S. Vignolini, J. J. Baumberg, *Sci. Adv.* **2019**, *5*, eaaw2205.
[34] J. Chen, Z. Wang, Z. Chen, S. Cong, Z. Zhao, *Nano Lett.* **2020**, *20*, 1915.
[35] Y. Lee, J. Yun, M. Seo, S. J. Kim, J. Oh, C. M. Kang, H. J. Sun, T. D. Chung, B. Lee, *Nano Lett.* **2020**, *20*, 6084.
[36] D. P. Puzzo, A. C. Arsenault, I. Manners, G. A. Ozin, *Angew. Chem., Int. Ed.* **2009**, *48*, 943.
[37] A. C. Arsenault, D. P. Puzzo, I. Manners, G. A. Ozin, *Nat. Photonics* **2007**, *1*, 468.
[38] I. Lee, D. Kim, J. Kal, H. Baek, D. Kwak, D. Go, E. Kim, C. Kang, J. Chung, Y. Jang, S. Ji, J. Joo, Y. Kang, *Adv. Mater.* **2010**, *22*, 4973.
[39] T. J. Park, S. K. Hwang, S. Park, S. H. Cho, T. H. Park, B. Jeong, H. S. Kang, D. Y. Ryu, J. Huh, E. L. Thomas, C. Park, P. E. T. Al, *ACS Nano* **2015**, *9*, 12158.
[40] S. Chen, S. Rossi, R. Shanker, G. Cincotti, S. Gamage, P. Kühne, V. Stanishev, I. Engquist, M. Berggren, J. Edberg, V. Darakchieva, M. P. Jonsson, *Adv. Mater.* **2021**, *33*, 2102451.
[41] T. Ding, *J. Mater. Chem. C* **2020**, *8*, 10825.
[42] M. A. Invernale, V. Seshadri, D. M. D. Mamangun, Y. Ding, J. Filloramo, G. A. Sotzing, *Chem. Mater.* **2009**, *21*, 3332.
[43] B. Lee, V. Seshadri, G. A. Sotzing, *Langmuir* **2005**, *21*, 10797.
[44] G. F. Castillo, G. Emilsson, A. Dahlin, *J. Phys. Chem. C* **2018**, *122*, 27516.
[45] E. Smela, N. Gadegaard, *Adv. Mater.* **1999**, *11*, 953.
[46] X. Wang, K. Chen, L. S. de Vasconcelos, J. He, Y. C. Shin, J. Mei, K. Zhao, *Nat. Commun.* **2020**, *11*, 211.
[47] J. Gladisch, E. Stavrinidou, S. Ghosh, A. Giovannitti, M. Moser, I. Zozoulenko, I. McCulloch, M. Berggren, *Adv. Sci.* **2020**, *7*, 1901144.
[48] T. Symmetrical, B. Lee, M. S. Yavuz, G. A. Sotzing, *Macromolecules* **2006**, *39*, 3118.
[49] N. Sharma, H. Keshmiri, X. Zhou, T. I. Wong, C. Petri, U. Jonas, B. Liedberg, J. Dostalek, *J. Phys. Chem. C* **2016**, *120*, 561.
[50] P. Hanarp, D. S. Sutherland, J. Gold, B. Kasemo, *Colloids Surf., A* **2003**, *214*, 23.
[51] H. Zhen, H. Ye, X. Liu, D. Zhu, H. Li, Y. Lu, Q. Wang, *Opt. Express* **2008**, *16*, 9595.
[52] M. F. Ponge, B. Dubus, C. Granger, J. O. Vasseur, M. P. Thi, A. C. Hladky-Hennion, *IEEE Transactions on Ultrasonics, Ferroelectrics, and Frequency Control* **2015**, *62*, 1114.
[53] R. Brooke, J. Edberg, X. Crispin, M. Berggren, I. Engquist, M. P. Jonsson, *Polymers* **2019**, *11*, 267.